Effects of thermal boundary conditions and cavity tilt on hydrothermal waves: Suppression of oscillations

R. Delgado-Buscalioni*

Departamento de Física Fundamental, UNED, Apartado 60141, Madrid 28080, Spain
(Received 10 October 2001; revised manuscript received 13 March 2002; published 12 July 2002)

Hydrothermal waves are longitudinal modes responsible for the onset of oscillations of low-Prandtl number flows inside end-heated cavities. We consider the flow induced by the hydrothermal wave in a rectangular enclosure whose differentially-heated side is tilted α degrees from the vertical position. An analytical approximation to the neutral curve and dispersion relation obtained by the Galerkin procedure is shown to quantitatively agree with the exact numerical solution of the stability problem. The analytical expressions are then used to dissect the effect of the Prandtl and Biot numbers and the inclination on the wave stability. In conducting walls the critical Rayleigh R_{cr} and wave number m_{cr} tend to a constant value at low Pr, while the critical frequency $f_{cr} \sim Pr^{-1/12}$. In adiabatic walls all these critical parameters increase like $Pr^{1/2}$. The boundaries can be considered to be poorly insulated if $Bi > Pr$, and in this case the critical parameters increase like $Bi^{1/2}$. On the other hand, R_{cr} and m_{cr} reach a minimum value at intermediate inclinations, while the critical frequency steadily increases with α. A closed equation for the frequency is also derived. This equation correctly forecasts the critical frequency in the unbounded domain and also the fundamental frequency measured in confined flows, as revealed by comparison with previous experiments and hereby presented numerical calculations for varying α. An important conclusion of the study is that for any arbitrarily small value of Pr the hydrothermal wave can be suppressed by heating the cavity above a theoretically predicted (Pr-dependent) angle. This prediction is of great relevance in the application domain (viz. the crystal growth from melts by the Bridgman technique).

I. INTRODUCTION

When a shallow cavity is filled with liquid metal and an externally imposed horizontal temperature difference is gradually increased, the thus created steady circulation can develop an oscillation generated by a longitudinal instability, commonly known as hydrothermal wave. This phenomena has been the subject of research over the past three decades. From a chronological standpoint, the active interest arises because of the relevance of this flow on the horizontal Bridgman technique, which is one of the most efficient ways for growing relatively large, high quality, homogeneous pure semiconductor crystals (see, e.g., [1]). Since the early experiments of Hurle *et al.* [2] it is known that the time-dependent flow induces thermal oscillations which in turn are some of the main reasons for the occurrence of undesirable striations, i.e., layered variations of impurities in the crystal. The relation between flow oscillations and crystal structure is still a subject of investigation (see, e.g. [3]). This fact addresses the necessity of a deeper understanding of the flow induced by the oscillatory longitudinal instability in order to eventually find possible ways to avoid or completely suppress it. The pioneer theoretical studies by Gill [4] and Hart [5,6] explained the basic physical origin of the oscillations showing that they occur in either gravitational and thermocapillary driven flows, taking energy by a coupling between momen-

tum and temperature perturbations with the mean shear and the basic driving force. Both authors provided analytical trends for the oscillation frequency in terms of the external and internal flow parameters. A point to be noted is that although the assumptions made in both theoretical works led to different frequency relationships (see Refs. [4] and [6]), the validity limits of the two theoretical trends has been scarcely further investigated in the literature. This point is revised in the present work.

Coming back to the problem addressed above, it should be mentioned that a common way to avoid the onset of oscillations is to apply a transversal magnetic field across the cavity. This fact also motivated a series of papers, starting from the pioneer experiments of Hurle *et al.* [2] to more recent numerical studies in Refs. [7,8] and stability analyses (see Ref. [9] and references therein). By such a procedure it is possible to delay the onset of oscillations towards larger temperature differences but pay the price of a severe reduction of the mean flow amplitude, and thus of the overall mass transport and crystal growth rates. Benz *et al.* [10] proposed another way for suppressing hydrothermal waves in thermocapillary-driven flows. Their method is based on heating troughs of low disturbance temperature (traced by a feedforward control scheme) with a sheet of infrared laser radiation.

Since the late 1980s, convection of low-Pr fluid in end-heated cavities was also thought to be a simple way for investigating possible routes to chaos in fluid dynamics. The linear stability analysis of the basic plane-parallel flow in the horizontal configuration was first studied by Hart [5,6], and then subsequently revised by Laure *et al.* [11] and by Kuo and Korpela [12] (insulated boundaries) and Wang and Korpela [13] (conducting walls). These studies showed that for

*Present address: Center for Computational Science, Department of Chemistry, Queen Mary, University of London, London E1 4NS, U.K. Email address: R.Delgado-Buscalioni@qmul.ack.uk; URL: www.fisfun.uned.es/~rafa

the range Prandtl number characteristic of liquid metals Pr $\sim 10^{-2}$, the oscillatory longitudinal instability is the most dangerous one, although its threshold is quite close to the onset of stationary transversal shear rolls (see [14] for a recent review). Several experiments were devoted to exploring the successive transitions towards aperiodic flow [15–17] and to characterizing the secondary Hopf bifurcations [18,19]. Numerical calculations of the three-dimensional flow are relatively more recent. These comprise the works in Refs. [21,22], concerning the flow at the transition to the periodic regime for one of the cases considered in Ref. [16]; and the study in Ref. [20], concerning the onset of the secondary Hopf-Hopf bifurcation.

In the case of upper free boundaries and Marangoni-driven flows, the analysis of Ref. [23] showed that the stability properties of the hydrothermal wave are rather sensible to the thermal behavior of the wall. Nevertheless, although it is not a simple task to achieve a perfectly insulating boundary under experimental conditions (see Ref. [16]), in the case of buoyancy-driven flows within rigid boundaries a similar investigation is not to be found in the literature. This investigation is part of the present work.

The inclination plays a crucial role on the mean flow structure [24]. For instance, it is known that extremely small, unavoidable inclinations ($\sim 0.5°$) can alter the crystal growth dynamics in the vertical Bridgman technique [25]. On the other hand, optimum tilting has been addressed as a feasible way to enhance the mass [26] and heat [24] transport rates, with direct application to the crystal growth technique [27]. Nevertheless, the effect of tilted boundaries on end-heated-enclosures flow instabilities received much less attention in the literature. A rather complete panorama of the adiabatic case can be found in Ref. [14], showing that the inclined setup makes feasible the study of several types of instabilities and their interactions or, alternatively, tilt may be used to suppress flow disturbances. In particular, this paper shows that a relatively easy way to suppress the oscillations induced by a hydrothermal wave is to tilt the cavity above a certain predicted inclination.

The rest of the paper can be summarized as follows. In Sec. II, the mean flow profiles are derived and Sec. III considers their stability with respect to oscillatory longitudinal modes. An equation for frequency is deduced in Sec. IV and used to dissect the relevance of the several processes affecting the oscillation for different external parameters. Section V discusses the effect of inclination and the effect of confinement is studied in Sec. VI by comparison with numerical calculations of the flow for varying Ra and inclination. Summary and concluding remarks are presented in Sec. VII.

II. GOVERNING EQUATIONS AND THE BASIC FLOW PROFILES

Let us consider the flow on the rectangular cavity of Fig. 1, whose dimensions along x, y, and z directions (width, depth, and length) are respectively $H=2h$, D, and L. The z axis is inclined an angle α with respect to the gravity vector, $\mathbf{g}=g\mathbf{e}_g$, with $\mathbf{e}_g=\sin(\alpha)\mathbf{i}-\cos(\alpha)\mathbf{k}$, and a temperature difference ΔT is imposed along the z axis. An incompressible fluid
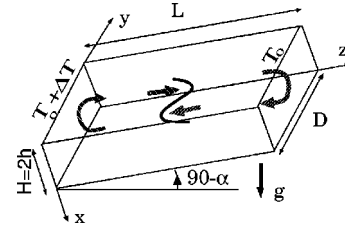
FIG. 1. Geometry of the problem and the basic mean stationary flow.

($\boldsymbol{\nabla}\cdot\mathbf{v}=0$) with thermal expansion coefficient β, kinematic viscosity ν, and thermal diffusivity κ fills the cavity and its motion is governed by the Navier-Stokes and heat transport equations with the Boussinesq approximation. The flow is determined by the following set of nondimensional parameters: the inclination, α, the aspect ratios, $A_z=H/L$ and $A_y=H/D$, the Rayleigh and Prandtl numbers, Ra $=g\beta\Delta Th^4/L\nu\kappa$ and Pr$=\nu/\kappa$, and the Biot number Bi which determines the thermal behavior of the lateral walls [see Eq. (3) below]. The Navier-Stokes and energy equations have been nondimensionalized by using Raκ/h, Ra$h(\Delta T/L)$, and $h^2/(\nu\kappa)^{1/2}$ as scales for velocity, temperature, and time, and $\rho_o g\beta(\Delta T/L)h^2\kappa^{1/2}/\nu^{1/2}$ for the pressure,

$$\frac{\partial \mathbf{v}}{\partial t}+\mathrm{Ra\,Pr}^{-1/2}\mathbf{v}\cdot\boldsymbol{\nabla}\mathbf{v}=-\boldsymbol{\nabla}P+\mathrm{Pr}^{1/2}\nabla^2\mathbf{v}-2A_z^{-1}\mathrm{RaPr}^{1/2}T\mathbf{e}_g,$$

$$\tag{1}$$

$$\mathrm{Pr}^{1/2}\frac{\partial T}{\partial t}+\mathrm{Ra}\mathbf{v}\cdot\boldsymbol{\nabla}T=\nabla^2 T. \tag{2}$$

The walls are rigid and the nonslip condition is assumed. The thermal boundary conditions at the $x=\pm H/2$ and $y=\pm D/2$ walls are the following ones,

$$\boldsymbol{\nabla}T\cdot\mathbf{n}+\mathrm{Bi}(T-T_{wall})=0, \tag{3}$$

where $\mathbf{n}$ is the unit vector normal to the surface of the walls and T_{wall} is the external temperature of the wall, decreasing linearly with the z coordinate. The Biot number appearing in Eq. (3) ranges from adiabatic, Bi$=0$, to perfectly conducting walls, Bi$=\infty$.

For any not vertical position the mechanical equilibrium is not possible and any externally imposed temperature difference leads to a clockwise unicellular steady circulation illustrated in Fig. 1. The flow at the core region is nearly plane parallel and turns around at the end regions placed at a distance of order $O(A_z)$ adjacent to the $z=\{0,2A_z^{-1}\}$ walls. The lateral walls at $y=\pm A_y^{-1}$ impose an even modulation in the flow amplitude which is only relevant at diffusive layers of thickness $O(A_y)$. In wide enough cavities ($A_y<1$) and away from these layers, one can neglect the flow y dependence and describe the basic circulation as a two dimensional steady flow in the $x-z$ plane. At the core region it is assumed that the basic flow can be described by a plane-parallel solution with the following structure,

$$\mathbf{v}=Kw_b(x)\mathbf{k},\qquad T=\frac{KA_z}{2}(z+\theta_b(x)+b), \tag{4}$$

where K is the ratio between the streamwise temperature gradient at the core and the externally imposed temperature gradient. By inserting Eq. (4) into the curl of Eq. (1) and into Eq. (2) one obtains a set of ordinary differential equations for the axial velocity and temperature x profiles. Their explicit analytical expressions depend on the local Rayleigh number at the core, $R = K\mathrm{Ra}$, and are shown in Table I.

The interested reader is referred to Ref. [24] for a comprehensive study of the steady flow and heat transfer regimes in the tilted configuration. Briefly, the profiles in Table I are valid in the conductive and transition regime, i.e., at low and moderate Rayleigh number. At larger Ra the structure of the steady flow is transformed owing to the development of the boundary layer regime (BLR). Anyhow, the frontier of the BLR is far above the range of values of Ra at which the hydrothermal wave appears (see Ref. [14]). To conclude with this section, an important point has to be mentioned about the dependence of the local Rayleigh number at the core R with the external Rayleigh number, Ra. The basic profiles for $\alpha < 90°$ in Table I diverge at a discrete set of values of R, the lowest one being $R_0/\cos\alpha$. As shown in Ref. [24], consideration of the closing walls at $z = \{0, L/h\}$ leads to the following conclusion: as Ra increases, the value of R asymptotically tends to the divergence value, in such a way that $R < R_0/\cos\alpha$. Hence, the limit $R \to R_0/\cos\alpha$ corresponds to the limit of infinite Rayleigh number, Ra $\to \infty$. Respectively for adiabatic and conducting walls, $R_0 = 31.28$ and $R_0 = \pi^4$.

III. EQUATIONS FOR THE PERTURBATIVE FLOW

In order to investigate the stability of the basic flow at the core region, it is convenient to choose the local temperature z gradient at the core $K\Delta T/L$ in the temperature scaling. Thus, the scale of velocity and temperature in the perturbation equations are respectively $R\kappa/h$ and $(R\Delta T/L)h$, and the basic velocity and temperature fields are now $\mathbf{v} = w_b(x)\mathbf{k}$ and $T_b = -z + \theta_b(x)$. As usual, the linearized equations for the perturbative flow are obtained by expressing each flow variable as the sum of the mean flow quantity and a small perturbation, inserting them into Eqs. (1) and (2) and neglecting products of perturbative quantities. We are hereby interested in oscillatory longitudinal perturbations whose motion can be described by the perturbative temperature, T_p, the streamwise component of the perturbative velocity, w_p, and one stream function Ψ_p for the flow in the $x - y$ plane: $\partial\Psi_p/\partial y = -u_p$ and $\partial\Psi_p/\partial x = v_p$. In the unbounded limit $A_z \to 0$ and $A_y \to 0$ the set of equations for the longitudinal perturbations is of the form $\mathcal{L}\mathbf{\Phi_p} = \mathbf{0}$, where

$$\mathcal{L} = \begin{pmatrix} \dfrac{\partial}{\partial t}\nabla^2 + \mathrm{Pr}^{1/2}\nabla^4 & 0 & -R\,\mathrm{Pr}^{1/2}\sin(\alpha)\dfrac{\partial}{\partial y} \\[3mm] -\dfrac{\partial}{\partial y}R\,\mathrm{Pr}^{-1/2}w_b' & \dfrac{\partial}{\partial t} - \mathrm{Pr}^{1/2}\nabla^2 & -R\,\mathrm{Pr}^{1/2}\cos(\alpha) \\[3mm] -R\theta_b'\dfrac{\partial}{\partial y} & -1 & \mathrm{Pr}^{1/2}\dfrac{\partial}{\partial t} - \nabla^2 \end{pmatrix} \tag{5}$$

with the following boundary conditions:

$$\Psi_p(\pm 1, y, t) = \frac{\partial\Psi_p}{\partial x}(\pm 1, y, t) = 0, \tag{6}$$

$$w_p(\pm 1, y, t) = 0, \tag{7}$$

$$T_p(\pm 1, y, t) \pm \mathrm{Bi}\frac{\partial T_p}{\partial x}(\pm 1, y, t) = 0. \tag{8}$$

For a given set of parameters $(R, m, \mathrm{Pr}, \alpha, \mathrm{Bi})$, the solution of Eqs. (5)–(8) is a vector, $\mathbf{\Phi}_p = (w_p, \Psi_p, T_p)$, with the following functional form

$$\mathbf{\Phi}_p(x, y, t) = \hat{\mathbf{\Phi}}_p(x)e^{imy + \Omega t}, \tag{9}$$

where $\hat{\mathbf{\Phi}}_p(x)$ is the array of perturbative amplitude (complex) functions. Inserting Eq. (9) into Eqs. (5)–(8) one obtains an eigenvalue problem for the complex growth rate, $\Omega = \Omega_r + i\Omega_i$. The resulting system was solved by a Tau-Chebyshev method. Accuracies of about 1% in both the eigenvalues and the eigenvectors were ensured by using a large enough number of basis functions which typically varied from $N = 15$ for low Pr < 0.05 to $N = 25$ for larger Pr and larger inclinations (see Ref. [28] for convergence details). For $\alpha = 90°$ (horizontal enclosures) the values of the critical Rayleigh number, critical wave number, and critical frequency differed by less than 2% to those reported in previous works [11,12]. The interested reader is referred to Ref. [14] for a complete report on the flow stability (including transversal instabilities) in the case of tilted enclosures with adiabatic walls and to Ref. [28] for the conducting counterpart.

A. Analytical approach

The Galerkin method has been used to obtain an analytical approximation to the eigenvalue problem arising from Eqs. (5)–(8). The accuracy of this method greatly depends on the choice of the trial functions. First, the trial functions have to satisfy the boundary conditions of Eqs. (6)–(8) and secondly they have to resemble as much as possible the perturbative amplitudes of the neutral mode. The amplitude functions have been modeled as $\hat{\mathbf{\Phi}}_p(x)$

TABLE I. Axial velocity and temperature basic profiles corresponding (respectively from top to bottom) to $0°<\alpha\leq90°$, $\alpha=90°$ and $90°<\alpha\leq180°$. The parameter r is defined as $r\equiv(R\cos\alpha)^{1/4}$ for $0°<\alpha<90°$ and $r\equiv(1/\sqrt{2})(-R\cos\alpha)^{1/4}$ for $90°<\alpha<180°$.

$$w_b(x)=\frac{\sin(\alpha)r^{-2}(1+\mathrm{Bi})[\sin(r)\sinh(rx)-\sin(rx)\sinh(r)]}{2\mathrm{Bi}\sin(r)\sinh(r)+r[\cosh(r)\sin(r)+\cos(r)\sinh(r)]}$$

$$\theta_b(x)=\frac{\sin(\alpha)}{r^4}\left(x-\frac{(1+\mathrm{Bi})[\sin(rx)\sinh(r)+\sin(r)\sinh(rx)]}{2\mathrm{Bi}\sin(r)\sinh(r)+r[\cosh(r)\sin(r)+\cos(r)\sinh(r)]}\right)$$

$$w_b(x)=\tfrac{1}{6}(-x+x^3)$$

$$\theta_b(x)=-\frac{(15+7\mathrm{Bi})x}{360(1+\mathrm{Bi})}+\frac{x^3}{36}-\frac{x^5}{120}$$

$$w_b(x)=\frac{\sin(\alpha)}{r^2}\frac{(1+\mathrm{Bi})[\mathcal{SCh}(r)\mathcal{CSh}(rx)-\mathcal{CSh}(r)\mathcal{SCh}(rx)]}{\mathcal{D}(r)}$$

$$\theta_b(x)=\frac{\sin(\alpha)}{4r^4}\left(x-\frac{(1+\mathrm{Bi})[\mathcal{SCh}(r)\mathcal{SCh}(rx)+\mathcal{CSh}(r)\mathcal{CSh}(rx)]}{\mathcal{D}(r)}\right)$$

$$\mathcal{CCh}(x)=\cos(x)\cosh(x),\quad \mathcal{SCh}(x)=\sin(x)\cosh(x),\ \text{etc}$$

$$\mathcal{D}(r)=r[\cos(r)\sin(r)+\cosh(r)\sinh(r)]$$
$$+\mathrm{Bi}[\cosh(r)^2\sin(r)^2+\cos(r)^2\sinh(r)^2]$$

$=(\bar{\Psi}_p F_\Psi(x),\bar{w}_p F_w(x),\bar{T}_p F_T(x))$ where $\mathbf{F}_\Phi(x)$ $=(F_\Psi(x),F_w(x),F_T(x))$ is a set of normalized functions and $\bar{\mathbf{\Phi}}_p=(\bar{\Psi}_p,\bar{w}_p,\bar{T}_p)$ is an array of complex numbers. The results presented in this paper were obtained with the following set of trial functions:

$$F_\Psi(x)=\sqrt{\frac{2}{3}}(1+\cos\pi x),\tag{10}$$

$$F_w(x)=F_\Psi(x),\tag{11}$$

$$F_T(x)=\frac{1}{\sqrt{c}}\left(1+d_T\cos(\pi x)+\frac{2}{\pi}(1-d_T)\mathrm{Bi}\cos\left(\frac{\pi}{2}x\right)\right).\tag{12}$$

The proposed trial functions have been normalized according to the scalar product $\langle F^2\rangle\equiv(1/2)\int_{-1}^{1}F^2(x)dx$ [in particular, $\langle F_T^2\rangle=1$ determines the constant c appearing in Eq. (12)]. The proposed amplitude for the perturbative temperature in Eq. (12) deserves a separate comment. For $\mathrm{Bi}\to\infty$, it simply becomes $F_T(x)=\cos(\pi x/2)$, while for low Bi (nearly insulating boundaries) it depends on the parameter d_T, which models the amount of heat diffused along the cross-stream direction [e.g., $F_T=1+d_T\cos(\pi x)$ for $\mathrm{Bi}=0$]. For any given values of the external parameters it is possible to calculate the *critical* value of d_T by requiring the minimization of the marginal Rayleigh number R_m in the plane (m,d_T). Alternatively, as long as $F_T''/F_T=-\pi^2 d_T^2+O(d_T^3)$, for any given perturbative temperature field T_p, the value of d_T can be estimated by means of, $\pi^2 d_T^2=-\langle T_p^{-1}\partial^2 T_p/\partial x^2\rangle$, where $\langle\cdot\rangle$ denotes the average along x and y-directions. It is advanced that the value of d_T for the critical perturbative temperature field is vanishingly small for $\mathrm{Bi}\simeq0$ and $\mathrm{Pr}<0.1$ [see

Fig. 3(a)]. Consequently, the rate of energy diffusion along the x direction shall be neglected in the foregoing analysis on the low-Prandtl range and adiabatic walls.

Inserting the functions defined in Eqs. (9)–(12) into the system (5), multiplying the resulting equations by $\mathbf{F}_\Phi e^{-im-\Omega t}$, and taking the scalar product leads to the following set of equations for $\bar{\mathbf{\Phi}}_p=(\bar{\Psi}_p,\bar{w}_p,\bar{T}_p)$

$$\langle\mathbf{F}_\Phi^T|\mathbf{L}\cdot\mathbf{F}_\Phi\rangle\cdot\bar{\mathbf{\Phi}}_p=0,\tag{13}$$

where $\mathbf{L}$ denotes the resulting operator in the x coordinate. Upon averaging, the diffusion operators are transformed into the following scalar form

$$\langle\mathbf{F}_\Phi^T|\nabla^2\mathbf{\Phi}\rangle=(\langle\mathbf{F}_\Phi|F_\Phi''\rangle-m^2\mathbf{1})\bar{\mathbf{\Phi}}_p\equiv-\mathbf{n}_\Phi^{(2)}\bar{\mathbf{\Phi}}_p,\tag{14}$$

where the array $\mathbf{n}_\Phi^{(2)}=(n_w^{(2)},n_\Psi^{(2)},n_T^{(2)})$ is composed of positive real numbers. Similarly, the ∇^4 operator appearing in the equation for the perturbative stream function on Eq. (5) is converted to $\langle F_\Psi|\nabla^4\Psi\rangle=n_\Psi^{(4)}\bar{\Psi}_p$ with $n_\Psi^{(4)}\equiv\langle F_\Psi|F_\Psi^{IV}\rangle-2m^2\langle F_\Psi|F_\Psi''\rangle+m^4>0$. For $d_T=0$ the scalars representing the diffusion operators are

$$n_w^{(2)}=n_\Psi^{(2)}=\frac{\pi^2}{3}+m^2,\tag{15}$$

$$n_\Psi^{(4)}=\frac{\pi^4}{3}+\frac{2\pi^2}{3}m^2+m^4,\tag{16}$$

$$n_T^{(2)}=\frac{\pi^2}{4}\left(\frac{2\mathrm{Bi}^2+4\mathrm{Bi}}{2\mathrm{Bi}^2+8\mathrm{Bi}+\pi^2}\right)+m^2,\tag{17}$$

while for $d_T>0$ and $\mathrm{Bi}=0$, $n_T^{(2)}=d_T^2\pi^2/2+m^2$.

The following real numbers shall also be needed: $c_{\Psi,T} = \langle F_\Psi | F_T \rangle = c_{w,T} = \langle F_w | F_T \rangle$. The value of c_{wT} ranges from $c_{wT} = 0.816$ for Bi $= 0$ (and $d_T = 0$) to $c_{wT} = 0.980$ for Bi $\rightarrow \infty$. The cross-stream gradient of the mean velocity and temperature appearing in Eq. (5) are transformed into the following averaged quantities: $\widehat{w_b'} = \langle F_w(x) w_b'(x) F_\Psi(x) \rangle < 0$ and $\widehat{\theta_b'} = \langle F_T(x) \theta_b'(x) F_\Psi(x) \rangle < 0$.

The characteristic equation arises from the solvability condition of the homogeneous system in Eq. (13): $\det[\langle \mathbf{F}_\Phi^T | \mathbf{L} \cdot \mathbf{F}_\Phi \rangle] = 0$. The present analysis is focused on longitudinal oscillatory marginal perturbations, so the complex growth rate can be set to a purely imaginary number $\Omega = i 2\pi f$, the oscillation frequency being f. Combining the imaginary and real part of the characteristic equation yields the neutral curve, $R_m = R_m(m; \text{Pr}, \alpha, \text{Bi})$ and the dispersion relation. For the sake of brevity, only the imaginary part of the characteristic equation is given:

$$(2\pi f)^2 = n_T^{(2)} \left(\frac{n_\Psi^{(4)}}{n_\Psi^{(2)}} + n_w^{(2)} \right) + \frac{n_\Psi^{(4)} n_w^{(2)}}{n_\Psi^{(2)}} \text{Pr} - \frac{c_{\Psi T}^2}{n_\Psi^{(2)}} R_m^2 m^2 \widehat{\theta_b'} \sin\alpha$$
$$- c_{wT}^2 R_m \cos\alpha. \qquad (18)$$

Let us now focus on the horizontal configuration to study the role of thermal boundary conditions and of the Prandtl number (the effect of leaning is deferred to Sec. V). The expression for the neutral curve for $\alpha = 90°$ is

$$\frac{R^2 m^2 c_{wT}^2}{n_\Psi^{(2)}} \left[|\widehat{w_b'}| - |\widehat{\theta_b'}| \left(\frac{n_\psi^{(4)}}{n_\Psi^{(2)}} \text{Pr} + n_T^{(2)} \right) \right]$$
$$= \left(\frac{n_\Psi^{(4)}}{n_\Psi^{(2)}} + n_w^{(2)} \right) \left(n_T^{(2)2} + n_T^{(2)} \frac{n_\Psi^{(4)}}{n_\Psi^{(2)}} \text{Pr} + n_w^{(2)} \frac{n_\Psi^{(4)}}{n_\Psi^{(2)}} \text{Pr}^2 \right).$$
$$(19)$$

The right-hand side (RHS) of Eq. (19) accounts for the overall diffusion. Note that in nondimensional units, the momentum and temperature diffusion are respectively $\text{Pr}^{1/2}$ and $\text{Pr}^{-1/2}$. The LHS of Eq. (19) reflects the "effective" driving mechanism of the oscillatory longitudinal modes, discussed in Refs. [4,6,14]. Owing to the imposed streamwise temperature gradient, any wavy z-velocity perturbation creates temperature fluctuations along the y direction, at a rate that can be estimated by averaging in Eq. (5), $d\langle T_p \rangle / dt \sim \text{Pr}^{-1/2} \langle w_p \rangle$. The fluctuation of buoyancy accelerates the fluid parcels along the x direction. The Ψ_p part of Eq. (5) leads to $d\langle u_p \rangle / dt \sim (R \, \text{Pr}^{1/2} m^2 / n_M^{(2)}) \langle T_p \rangle$. Owing to the mean shear, the cross-stream current activates a stress force along the z direction, pulling against the initial velocity perturbation, which decreases at a rate $d\langle w_p \rangle / dt \sim R \, \text{Pr}^{-1/2} |\widehat{w_b'}| \langle u_p \rangle$ and finally reverts its motion around a quarter of the cycle. The sign of the perturbative temperature field (and the buoyant force along the x direction) are thus inverted by the streamwise advection and the same reasoning applies for the rest of the cycle. Successive time derivation on the above rates leads to $\langle w_p \rangle^{-1} d^3 \langle w_p \rangle / dt^3 \sim R^2 m^2 \text{Pr}^{-1/2} |\widehat{w_b'}| / n_\Psi^{(2)}$,

which represents the rate of the basic restoring mechanism (to the third power), appearing in the first term on the LHS of Eq. (19). The second term on the LHS of Eq. (19) represents the reduction of the restoring force due to heat advection along x direction. This current carries cold fluid from the bottom surface ($x = 1$) to regions with excess of temperature (and vice versa) at a rate $R |\widehat{\theta_b'}| \langle u_p \rangle$ and reduces the buoyant force along the x direction. This mechanism is able to damp out the oscillation if the diffusion of temperature is slow enough. This corresponds to the vanishing of the LHS of Eq. (19): $\text{Pr} > (|\widehat{w_b'}| / |\widehat{\theta_b'}| - n_T^{(2)}) (n_\Psi^{(2)} / n_\Psi^{(4)})$. It is advanced (see Sec. V) that the hydrothermal wave can also be inhibited at arbitrarily small Pr and large enough inclinations, as a consequence of the streamwise stratification.

For any value of the external parameters the critical wave number lies within the range $m \leq O(1)$. Hence a fourth order expansion of $R_m^2 m^2$ around $m = 0$ [taken from Eq. (19)] provides rather accurate values of the critical Rayleigh number and wave number. Such expansion reads

$$R_m^2 m^2 = a_{-2} + a_0 m^2 + a_2 m^4 + \text{h.o.t.}, \qquad (20)$$

where the coefficients a_{-2}, a_0 and a_2 are independent on the wavelength and are straightforward calculated from Eq. (19). Equation (20) provides the following expressions:

$$m_{cr} = \left(\frac{a_{-2}}{a_2} \right)^{1/4}, \qquad (21)$$

$$R_{cr} = (a_0 + 2\sqrt{a_{-2} a_2})^{1/2}. \qquad (22)$$

Some insight on the wave number selection can be obtained from Eqs. (20) and (21). Large structures, with $m < m_{cr}$, become unstable if the effective source of instability ($\propto R^2 m^2$) overpowers a certain cross-stream diffusion rate, determined by a_{-2}. Hence, at the long-wave limit, $R_m \simeq \sqrt{a_{-2}} m^{-1}$. On the other hand, the diffusion of small structures ($m > m_{cr}$) occurs along the y direction and it is governed by the term $a_2 m^4$; in particular $R_m \simeq \sqrt{a_2} m$ for $m > m_{cr}$. The critical wave number satisfies $a_2 m_{cr}^4 = a_{-2}$, indicating that the selected wavelength establishes a balance between the overall diffusion rates along x and y directions. This conclusion shall be used in the foregoing order of magnitude analyses to provide estimations of the critical wave number in different scenarios.

Figure 2 compares the critical parameters obtained from the single-term Galerkin expansion with the exact ones arising from the numerical solution Eqs. (5)–(8). Considering the simplicity of the analytical approach, the agreement is quite remarkable particularly in the case of conducting boundaries, for which the analytical approach even provides a rather accurate prediction of the stabilizing value of the Prandtl number (Pr$\simeq 0.5$). In the case of adiabatic walls the analytical model works perfectly for Pr< 0.1, while the discrepancy at larger Pr (see Fig. 2) is a consequence of the failure of the $d_T = 0$ assumption. To show this fact the value of d_T has been plotted in Fig. 3(a) versus Pr. The sudden
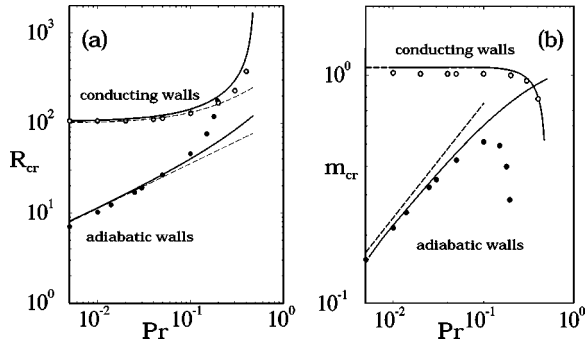
FIG. 2. (a) The critical Rayleigh number; (b) the critical wave number versus the Prandtl number. Points corresponds to the numerical solution of the linear stability problem and lines to the analytical approximation. Dashed lines are the asymptotic trends for Pr→0 in Eq. (23)–(28).

jump of the heat diffusion at Pr>0.1 clearly delimits the frontier for the low-diffusion assumption.

The effect of the thermal behavior of the walls on the stability properties is now discussed by means of order of magnitude analyses and of the asymptotic limits of the critical parameters extracted from the analytical expressions.

B. Adiabatic walls

For Pr≪1 the rate of cross-stream heat diffusion is very fast $O(\mathrm{Pr}^{-1/2})$ and the isothermals reach almost instantaneously the equilibrium profile. If a vanishing heat flux along the $x=\pm 1$ boundaries is imposed along $x=\pm 1$, the thermal equilibrium profile is the conduction solution along x [i.e., $d_T=0$ in Eq. (12)]. As a consequence, the input of energy by perturbative advection is uniquely diffused along the y direction at a rate $\Omega_\kappa^{(y)}\sim m^2\mathrm{Pr}^{-1/2}$. Under this situation momentum is the fastest diffused quantity along the x direction, $\Omega_\nu^{(x)}\sim\mathrm{Pr}^{1/2}$, and the critical wave number can be estimated by considering that the temperature spreading along the y direction is slaved to the momentum diffusion. Hence, $\Omega_\kappa^{(y)}\sim\Omega_\nu^{(x)}$ and $m_{cr}\sim\mathrm{Pr}^{1/2}$. An estimation of the prefactor can be
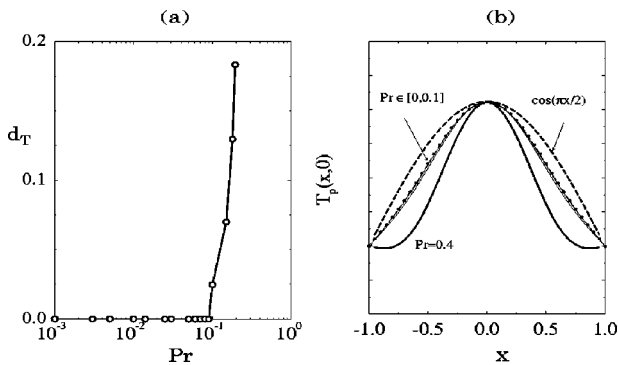
FIG. 3. (a) The value of the parameter d_T measured at $\alpha=90°$ according to $\pi^2 d_T^2=-\langle T_p^{-1}\partial^2 T_p/\partial x^2\rangle$, T_p being the critical temperature perturbation in adiabatic walls. (b) Perturbative temperature x profiles in the case of conducting boundaries and $\alpha=90°$. Dashed line corresponds to the perturbation assumed by the analytical model [see Eq. (12)].

obtained using the proposed perturbative field on Eqs. (9)–(12): $\Omega_\nu\simeq(\pi^2/3)\mathrm{Pr}^{1/2}$ and $\Omega_\kappa\simeq m^2\mathrm{Pr}^{-1/2}$. This provides $m_{cr}\simeq 1.8\,\mathrm{Pr}^{1/2}$, very close to the trend extracted from the exact numerical solution of Eqs. (5): $m_{cr}=2.2\,\mathrm{Pr}^{1/2}$. The solution of Eq. (20) deviates by less than 8% to the former trend,

$$m_{cr}=2.38\,\mathrm{Pr}^{1/2}+O(\mathrm{Pr}^{3/2}), \tag{23}$$

$$R_{cr}=112\,\mathrm{Pr}^{1/2}+O(\mathrm{Pr}^{3/2}). \tag{24}$$

The critical frequency can be obtained from Eq. (18),

$$2\pi f_{cr}=10.3\,\mathrm{Pr}^{1/2}+O(\mathrm{Pr}^{3/2}). \tag{25}$$

As shown in Eq. (25), the critical frequency is of the same order (although slightly greater) than the effective rate of heat and momentum diffusion $[\Omega_\nu^{(x)}\simeq\Omega_\kappa^{(y)}\simeq(\pi^2/3)\mathrm{Pr}^{1/2}]$. It is noted that in adiabatic walls the rate of perturbative heat advection along the x direction $[u_p R|\widehat{\theta_b'}|\sim O(\mathrm{Pr})]$ can be neglected, as it is smaller than the dominant diffusion rate, $\Omega_\nu^{(x)}\sim\mathrm{Pr}^{1/2}$. This fact can also be seen from Eq. (19). As shown afterwards this fact does not hold in the case of conducting boundaries.

C. Perfectly conducting boundaries

The previously described situation is completely changed if a certain amount of energy flux is imposed through the $x=\pm 1$ walls. In this case a part of the energy supplied by streamwise advection at the central part of the layer has necessarily to be diffused along the x direction in order to maintain the wall's temperature constraints. As long as at low Pr energy it is much more rapidly diffused than momentum, the fastest diffusion rates along the x and y direction are respectively $\Omega_\kappa^{(x)}\simeq(\pi^2/4)\mathrm{Pr}^{-1/2}$ and $\Omega_\kappa^{(y)}\simeq m^2\mathrm{Pr}^{-1/2}$. As previously concluded the critical disturbance enables the balance of the diffusion rates along these two directions; therefore $m_{cr}\simeq\pi/2$. In the case of conducting walls, the above reasoning is equivalent to considering that the critical perturbation minimizes the amount of heat diffused out of each perturbative cell, which is proportional to $\int_{-1}^{1}\int_{-\pi/2m}^{\pi/2m}\nabla^2 T_p dx dy$. In fact, for the perturbative temperature proposed in Eqs. (9) and (12), this integral minimizes for $m=\pi/2$. This estimation can now be compared to the asymptotics obtained from Eq. (20) (which agree within ~3% with the exact ones for Pr<0.05; see Fig. 2),

$$m_{cr}=1.08+0.48\,\mathrm{Pr}+O(\mathrm{Pr}^2), \tag{26}$$

$$R_{cr}=99.27++317.07\,\mathrm{Pr}+O(\mathrm{Pr}^2), \tag{27}$$

$$2\pi f_{cr}=9.40+28.16\,\mathrm{Pr}+O(\mathrm{Pr}^2). \tag{28}$$

Note that the critical wave number is somewhat smaller ($m_{cr}\simeq 1$) than predicted by the minimization of heat diffusion. The reason is that the critical perturbation tends to further reduce the wave number to lessen the stabilizing effect of the cross-stream heat advection. This fact can be seen by solving Eq. (19) with an artificially imposed vanishing value of $|\widehat{\theta_b'}|$, resulting in $m_{cr}=1.5$ and $R_{cr}=79$. In conducting walls it turns out that $n_T^{(2)}\sim O(1)$, so the cross-stream advec-

tion has a sizeable stabilizing contribution in the neutral curve of Eq. (19) even at $\mathrm{Pr} \to 0$. This result counterpoints with the adiabatic case.

D. The effect of Biot number

Let us first consider the case of nearly adiabatic walls ($\mathrm{Bi} \ll 1$). As stated earlier, irrespective of the wall thermal behavior, the rate of heat diffusion along the y direction is $\mathrm{Pr}^{-1/2} m^2 \bar{T}_p$. On the other hand, for a small Biot number a certain drop of perturbative temperature sets up along the cross-stream direction. The heat diffusion rate can be estimated from Eqs. (9) and (12): $\langle \partial^2 T_p / \partial x^2 \rangle = (\pi/2) \mathrm{Pr}^{-1/2} \mathrm{Bi} \bar{T}_p$. Now, if heat is the fastest diffused quantity along the x direction the wave number selection is determined from the balance of heat diffusion rates, as in the conducting case, leading to $m_{cr} \sim \mathrm{Bi}^{1/2}$. Nevertheless, for $\mathrm{Bi} < O(\mathrm{Pr})$, the rate of momentum diffusion $O(\mathrm{Pr}^{1/2})$ overpowers that of heat diffusion $O(\mathrm{Pr}^{-1/2} \mathrm{Bi})$, and the trend for perfectly insulating boundaries is recovered. According to the asymptotic solution of Eq. (19), shown in Eqs. (29)–(31), the nearly adiabatic limit is recovered for $\mathrm{Bi} < 5\,\mathrm{Pr}$ (see also Fig. 4). Up to $O(\mathrm{Bi}^{-3/2})$ and $O(\mathrm{Pr}^{3/2})$, one obtains

$$m_{cr} = \mathrm{Bi}^{1/2} + 2.38\,\mathrm{Pr}^{1/2}, \tag{29}$$

$$R_{cr} = 45.29\{\mathrm{Bi}^{1/2} + 2.47\,\mathrm{Pr}^{1/2}\}, \tag{30}$$

$$\Omega_{cr} = 5.13\{\mathrm{Bi}^{1/2} + 2.02\,\mathrm{Pr}^{1/2}\}. \tag{31}$$

Let us now consider the case of quasiperfectly conducting boundaries, i.e., $\mathrm{Bi}^{-1} \approx 0$. The expansion of the analytical trends around $\mathrm{Bi}^{-1} = 0$ leads to the following relations [valid up to $O(\mathrm{Bi}^{-3/2})$ and $O(\mathrm{Pr}^{3/2})$]:

$$m_{cr}^2(\mathrm{Bi}) = m_{cr}^2(\infty) - (0.66 - 6.60\,\mathrm{Pr})\mathrm{Bi}^{-1}, \tag{32}$$

$$R_{cr}^2(\mathrm{Bi}) = R_{cr}^2(\infty) - (4.3 10^4 - 2.6 10^4 \mathrm{Pr})\mathrm{Bi}^{-1}, \tag{33}$$

$$\Omega_{cr}^2(\mathrm{Bi}) = \Omega_{cr}^2(\infty) - (328.5 - 1408\,\mathrm{Pr})\mathrm{Bi}^{-1}. \tag{34}$$

As seen in Fig. 4, the trends (32)–(34) deviate by less than about 8% to the exact analytical solutions for $\mathrm{Bi} > 10$ and $\mathrm{Pr} < 0.1$.

IV. RELATION FOR THE FREQUENCY

Owing to the applications mentioned in Sec. I, the derivation of theoretical trends for the hydrothermal wave frequency has been an important part of the endeavor of the previous theoretical analyses, as those by Gill [4] and Hart [6]. Surprisingly, although both authors proposed different theoretical descriptions and frequency trends for the $\mathrm{Pr} \to 0$ limit, any study concerning the validity range of both approaches is found among the relative abundant literature on this topic. In this section an equation is derived for the frequency which recovers Hart's and Gill's trends at the limit of slow and fast energy diffusion. The equation extends the previous analysis depicted in Ref. [14] by taking into account the effect of heat and momentum diffusion and of the cross-stream advection.

To begin with, we proceed as in Ref. [14]. Consider that a
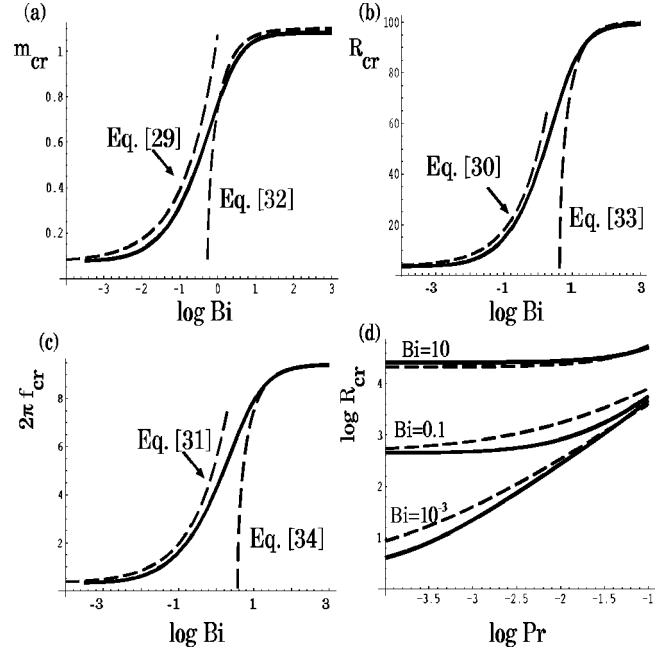
FIG. 4. (a) The dependence of the critical wave number, (b) critical Rayleigh number, and (c) critical frequency with the Biot number for $\mathrm{Pr} = 0.025$ and horizontal cavities, $\alpha = 90°$ and $\mathrm{Pr} = 10^{-3}$. (d) corresponds to the critical Rayleigh number. Dashed lines in (d) correspond to Eq. (30) ($\mathrm{Bi} = 10^{-3}$ and 0.1) and Eq. (33) ($\mathrm{Bi} = 10$).

positive disturbance of velocity along the z axis is made at an instant t_0 and around $y = 0$. The subsequent evolution of the perturbative flow can be represented by taking the real part of Eqs. (9),

$$w_p(x,y;t) \simeq F_w(x)\cos(my)\tilde{w}_p(t),$$

$$\Psi_p(x,y;t) \simeq F_\Psi(x)\sin(my)\tilde{u}_p(t), \tag{35}$$

$$T_p(x,y;t) \simeq F_T(x)\cos(my)\tilde{T}_p(t).$$

The time-dependent part of the perturbation has been introduced in functions like $\tilde{w}_p(t)$ and the initial condition of the perturbation is $\tilde{w}_p(t_0) > 0$. The perturbative flow at a time $t = \delta t$ shall be described expanding to first order in time the equations for the longitudinal disturbances [Eqs. (5)] averaged according to Eq. (13). This leads to

$$\mathrm{Pr}^{1/2}\tilde{T}_p + n_T^2 \tilde{T}_p \delta t = \tilde{w}_p(t_0)\delta t, \tag{36}$$

$$(\mathrm{Pr}^{1/2} n_\Psi^{(2)}\delta t + 1)\tilde{u}_p = -\frac{m^2 R\,\mathrm{Pr}^{1/2}\sin\alpha}{n_\Psi^{(2)}}\tilde{T}_p\delta t, \tag{37}$$

$$(\mathrm{Pr}^{1/2} n_\Psi^{(2)}\delta t + 1)\tilde{w}_p = \tilde{w}_p(t_0) + \tilde{u}_p \widehat{|w_b'|}R\,\mathrm{Pr}^{-1/2}\delta t$$
$$+ R\,\mathrm{Pr}^{1/2}\cos\alpha\,\delta t. \tag{38}$$

For the sake of simplicity we have introduced $n_M^2 \equiv n_\Psi^{(2)} = n_w^{(2)}$ and we have chosen $n_M^4 = n_\Psi^{(4)}$ in Eq. (37). Although this choice is incoherent with the shape of F_Ψ in Eq. (10), it

TABLE II. Order of magnitude of the several frequencies appearing in Eq. (39). Frequencies are in units of $(\nu\kappa)^{1/2}/h^2$. The contribution of f_{BV} is discussed in Sec. V

B.C.	f_{cr}	f_κ	f_ν	f_{adv}	f_{Gill}	f_{Hart}
$Bi=0$	$1.6\,Pr^{1/2}$	$1.2\,Pr^{1/2}$	$0.8\,Pr^{1/2}$	$O(Pr)$	$O(Pr^{1/2})$	$O(Pr^{1/2})$
$Bi\rightarrow\infty$	1.6	$0.8\,Pr^{-1/2}$	$Pr^{1/2}$	$O(1)$	$O(1)$	$O(Pr^{-1/6})$

introduces almost no variation on the results. Inserting Eq. (36) into Eq. (38) and the resulting equation into Eq. (37) one obtains a closed expression for $\widetilde{w}_p(t)$ up to δt^3. The resulting expression can then be used to obtain an estimation of the frequency. The value of $\widetilde{w}_p$ changes sign at a quarter of a cycle; hence $\widetilde{w}_p=0$ around $\delta t=f^{-1}/4$. This reasoning leads to the following equation:

$$(f+f_\nu)^2\left(1+\frac{f}{f_\kappa}\right)=f_{Gill}^2+\frac{f}{f_\kappa}(\sigma f_{BV}^2-f_{adv}^2), \quad (39)$$

where

$$f_{Gill}\equiv\frac{c_{wT}}{4}\left(\frac{R^2m^2|w_b'|\sin\alpha}{n_M^2n_T^{(2)}}\right)^{1/2}, \quad (40)$$

$$f_{adv}\equiv\frac{c_{wT}}{4}\left(\frac{R^2m^2|\widehat{\theta_b'}|}{n_M^2}\sin\alpha\right)^{1/2}, \quad (41)$$

$$f_\kappa\equiv\frac{n_T^{(2)}}{4\,Pr^{1/2}}, \quad (42)$$

$$f_\nu\equiv\frac{n_M^2}{4\,Pr^{1/2}}, \quad (43)$$

$$\sigma f_{BV}^2\equiv\begin{cases}-\left(\dfrac{c_{wT}}{4}\right)^2R\cos\alpha & \text{for } \alpha<90°\\[2mm]\left(\dfrac{c_{wT}}{4}\right)^2R|\cos\alpha| & \text{for } \alpha>90°.\end{cases} \quad (44)$$

The newly introduced frequencies correspond to the following mechanisms: f_{Gill} represents the main oscillatory driving (see below); f_{adv} is the (stabilizing) contribution of the cross-stream advection which tends to diminish the frequency of oscillations; f_{BV} comes from the streamwise buoyancy and its effect shall be discussed in Sec. V. Finally f_κ and f_ν are proportional to the inverse of the characteristic heat and momentum diffusion times.

In previous theoretical analyses of the low-Prandtl-limit, the momentum diffusion has usually been neglected without justification (see e.g., [4,6,12]). It is remarked that such a simplification is only possible if the transient rate of momentum change is much larger than that associated with momentum dissipation, $f\gg f_\nu$. Although at low Pr this inequality holds for critical perturbations in conducting boundaries (see Table II), in adiabatic walls the contribution of momentum

diffusion has necessarily to be included in the frequency analysis because it turns out that $f_{cr}\sim f_\nu\sim O(Pr^{1/2})$ for any small value of Pr.

Depending on how the frequency f compares with the effective thermal diffusion rate f_κ two different possible situations arise, as revealed by inspection of Eq. (39). As explained in Ref. [14], if $f>f_\kappa$, the amount of energy diffused along each period of oscillation can be neglected and the transient variation of heat equals the rate of energy supplied by advection $[\partial T_p/\partial t=w_p]$. In the opposite case, $f<f_\kappa$, thermal diffusion distributes the advected heat much faster than the dynamic change of any flow quantity, so the temperature is in phase with the perturbative axial velocity $[\nabla^2 T_p=-w_p]$. It should be also remarked that the thermal effects at the RHS of Eq. (39) (f_{BV} and f_{adv}) are negligible only if the time needed to diffuse the temperature fluctuations is much shorter than the period of oscillation; i.e., if $f/f_\kappa\ll1$.

With these facts in mind, let us now revise the two theoretical approaches derived by Hart [6] and Gill [4] for the horizontal case and low Pr . It is recalled that in both theoretical works the contribution of the momentum diffusion was assumed negligible, and hence f_ν shall not be included in the following revision. The implication of this assumption on the adiabatic case is analyzed afterwards.

1. The case $f\ll f_\kappa$: Gill's assumption

The above inequality implies that one can neglect the terms accompanying the ratio f/f_κ in the RHS of Eq. (39), leading to $f=f_{Gill}$, where f_{Gill}, defined in Eq. (40), coincides (unless constant factor) with the solution obtained by Gill [4] for the formal $Pr\rightarrow0$ (R finite) limit of Eqs. (5)–(8). It is noted that f_{Gill} stands for the rate of variation of the driving oscillatory force in a highly conducting ($f_\kappa\gg f$) but inviscid ($f_\nu\ll f$) media.

2. The case $f\gg f_\kappa$: Hart's assumption

From Eq. (39), the above inequality leads to

$$f\approx[f_{Hart}-f(f_{adv}^2-f_{BV})]^{1/3}, \quad (45)$$

$$f_{Hart}\equiv\frac{c_{wT}}{4}\left(\frac{R^2m^2\sin\alpha Pr^{-1/2}|w_b'|}{n_M^2}\right)^{1/3}. \quad (46)$$

In the case of horizontal cavities with adiabatic walls and at low values of Prandtl number, the term f_{adv} is vanishingly small and Eq. (46) coincides (unless constant factor) with the trend proposed by Hart in Ref. [6]. It is stressed that the assumptions $f_\kappa\ll f$ and $f_\nu\ll f$ mean that the wave dynamics are not influenced by either momentum or energy diffusion.
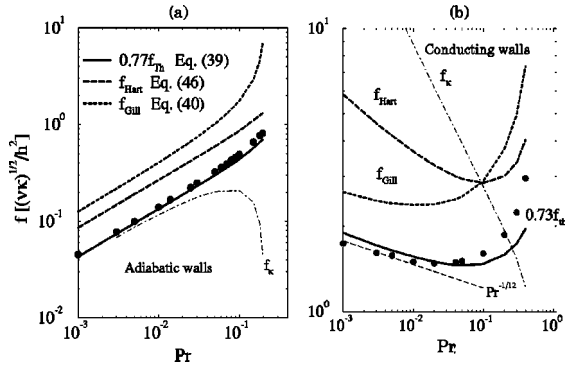
FIG. 5. The analytical frequency trends extracted from Eqs. (40), (46) (dashed lines) and Eq. (39) (solid line) compared with the critical frequency obtained from the numerical solution of the linear stability problem (circles). Data correspond to horizontal cavities ($\alpha = 90°$) in cavities with (a) adiabatic and (b) conducting walls.

In other words, f_{Hart} represents the rate of variation of the restoring force arising purely from the basic hydrothermal coupling and regardless of the delay induced by diffusive effects.

A. Adiabatic walls

As shown in Sec. III B, if the walls are perfectly insulating the critical parameters for the horizontal case go like $m_{cr} \simeq 2.2 \mathrm{Pr}^{1/2}$, $R_{cr} \simeq 10^2 \mathrm{Pr}^{1/2}$, and $f_{cr} \simeq 1.6 \mathrm{Pr}^{1/2}$. The orders of magnitude and estimations exposed in Table II are obtained by introducing these trends into Eqs. (40)–(43) (the prefactors are valid for $\alpha = 90°$).

Figure 5 compares the critical frequency obtained from the numerical solution of Eqs. (5)–(8) with the outcome of Eq. (39), Eq. (46) and Eq. (40), (respectively labeled as f_{th}, f_{Hart} and f_{Gill}). Concerning the adiabatic case [see Fig. 5(a)] the first point to be noted is that at low Pr, both f_{Hart} and f_{Gill} correctly line up with the slope $f_{cr} \sim \mathrm{Pr}^{1/2}$. As stated, in the adiabatic case $f_{cr} \sim f_\kappa$, so the critical perturbations lie just between the range of applicability of both Eqs. (46) and (40). Nevertheless none of these two trends properly take into account the finite diffusion rates and as a consequence both overvalue the critical frequency by a certain factor, which depends on the particular setup. For the critical perturbations these factors could be forecasted by using the estimations for f_ν, f_κ, and f_{cr} given in Table II. Note that $f_{cr} + f_\nu \simeq 1.51 f_{cr}$ and $f + f_\kappa \simeq 1.75 f_{cr}$; operating at the LHS of Eq. (39) leads to $f_{cr} \simeq 0.4 f_{Gill}$. Similarly, as $f_{Hart}^3 = f_\kappa f_{Gill}^2$, the LHS of Eq. (39) yields $f_{cr} \simeq 0.45 f_{Hart}$; both corrections being very close to f_{cr}.

As seen in Fig. 5, Eq. (39) provides better concordance with the absolute values of f_{cr}, as long as it takes into account heat and momentum diffusion. The critical frequency is anyhow slightly overestimated (the best fit corresponding to $f_{cr} \simeq 0.77 f_{th}$). Although this discrepancy could be surely reduced by further melioration of the constructed perturbative flow, it shall be shown that the ratio $f_{cr}/f_{th} = 0.75 \pm 0.05$ remains unaltered for $\mathrm{Pr} < 0.1$, irrespectively of the thermal boundary condition and inclination. Another proof of the consistency of Eq. (39) is given in Sec. VI, where it is

shown that the same ratio is obtained when comparing f_{th} with the frequency measured in numerical calculations and previous experiments in confined flows. These facts ensure that Eq. (39) can be used in the subsequent analysis.

B. Conducting boundaries

Using the critical parameters for the horizontal case, $R_{cr} \simeq 10^2$ and $m_{cr} \sim 1$, one obtains the estimations shown in Table II. In the conducting case $f_\kappa \gg f_{cr} \gg f_\nu$, so it is possible to neglect the contribution of the momentum diffusion in Eq. (39). Also as a first approximation one should use the infinitely fast heat diffusion assumption of Eq. (40), leading to $f_{Gill} \sim O(1)$. Indeed [see Fig. 5(b)], the infinitely slow heat diffusion limit $f_{Hart} \sim \mathrm{Pr}^{-1/6}$ clearly fails for the conducting case, whereas $0.7 f_{Gill}$ fits better to f_{cr} at low Prandtl number. Nevertheless, for $0 < \mathrm{Pr} < 0.02$, the exact values of the critical frequency scales like $f_{cr} \sim \mathrm{Pr}^{-1/12}$ [see Fig. 5(b)]. This slight variation means that the finite thermal diffusion rate still contributes at very low Pr, with a weak but appreciable delay. It is remarked that this effect was not reported in previous stability analysis [6,11,13] because the lowest values of Pr thereby considered were around 10^{-2}. As seen in Fig. 5(b), the outcome of Eq. (39) correctly reproduces this decreasing slope and fits to $f_{cr} \simeq 0.73 f_{th}$, in good agreement with the previous comparison for the adiabatic case. For $\mathrm{Pr} > 0.1$, the ratio f_{cr}/f_{th} increases as a consequence of a greater mismatch between the temperature profile assumed in Eq. (12) and the critical one. As seen in Fig. 3(b), just above Pr > 0.1, the ansatz $T_p \propto \cos(\pi x/2)$ largely underestimates the heat diffusion, which becomes more concentrated around $x = 0$. This mismatch leads to deviations with respect to f_{cr} by a certain factor which is essentially Pr dependent and does not greatly vary with the inclination [see Fig. 7(c)]. It is finally remarked that $\mathrm{Pr} > 0.1$ determines the frontier of low diffusion for both $\mathrm{Bi} \to \infty$ and $\mathrm{Bi} = 0$ [see Fig. 3(a)].

V. THE EFFECT OF INCLINATION

The amplitude of the effective restoring force that drives the instability is proportional to the x component of buoyancy, i.e., to $\sin \alpha$. Hence any tilt with respect to the horizontal position tends to increase the critical Rayleigh number and thus the critical frequency. Anyhow the effect of inclination is also strongly dependent on the other component of buoyancy which acts along the streamwise direction. Its role is now analyzed.

For $\alpha < 90°$ the unstable stratification along the streamwise direction favors perturbations with larger wavelengths. Concerning the critical Rayleigh number, it decreases for inclinations slightly smaller than $90°$ as a consequence of the larger mean flow velocities (see [24]). Anyhow, as seen in Fig. 6, below a certain tilt this trend is reverted and at low inclinations $R_{cr} \to R_0/\cos\alpha$, meaning that Ra_{cr} increases beyond bounds (see Sec. II). This is a consequence of the following mechanism: as far as $w_p T_p > 0$ along almost the entire cycle, the streamwise component of buoyancy always tends to maintain unaltered the sense of w_p. Therefore the effective restoring force (proportional to the mean shear) has
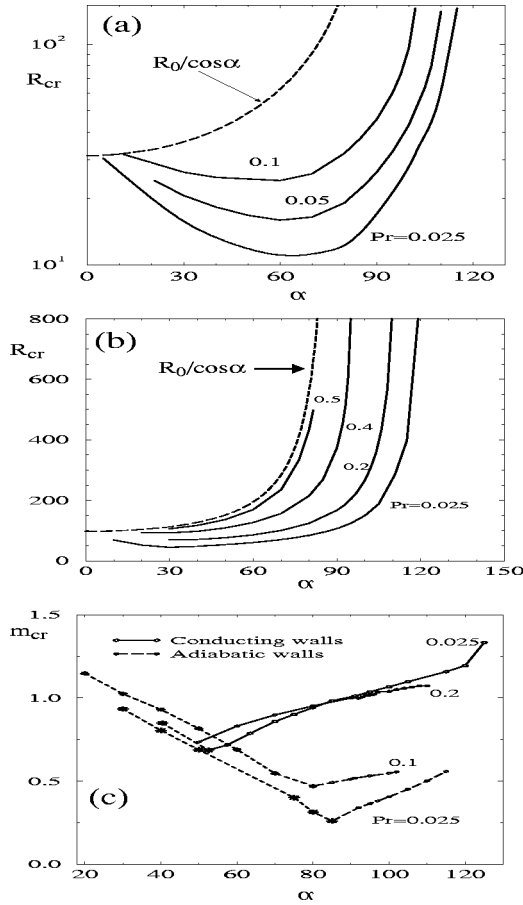
FIG. 6. The critical Rayleigh number for adiabatic (a) and conducting walls (b), and (c) the critical wave number versus the inclination angle. The dashed line in (a) and (b) corresponds to $R = R_0/\cos\alpha$, which stands at the limit Ra$\rightarrow\infty$. The value of R_0 is 31.28 and π^4 respectively for adiabatic and conducting walls.

FIG. 7. The critical frequency in the unbounded domain versus α. (a) and (b) correspond to Pr$=0.025$ and respectively Bi$\rightarrow\infty$ and Bi$\rightarrow0$, (c) to Pr$=0.2$ and Bi$\rightarrow\infty$, and (d) to Pr$=0.1$ and Bi$=0$. Circles correspond to the critical frequency f_{cr} obtained by numerical solution of the stability problem. Dashed lines correspond to the trends signaled at the above legends, and the solid lines correspond to the solution of Eq. (39), f_{Th}. In (a), (b) and (d) f_{Th} has been multiplied by 0.77.

to overpower the buoyant force in a part of the oscillation cycle. Two immediate consequences are that R_{cr} and the oscillation period increase for $\alpha<90°$ In Eq. (39) this is reflected in the negative contribution of f_{BV} to the frequency for $\alpha<90°$. At low enough inclinations the streamwise perturbative flow can no longer be reverted and, as shown in Ref. [14], the oscillatory mode is damped in favor of a (Rayleigh-Bénard-like) stationary longitudinal roll, driven by the streamwise buoyant force. The points marked with star symbols in Fig. 6(c) are placed on the smallest wave number for which the oscillatory longitudinal modes can become unstable.

If the cavity is heated from above ($\alpha>90°$) the streamwise buoyancy acts within a completely stable stratification whose effect is to further increase R_{cr}. On the other hand, the restoring torque along the x direction generated by the streamwise buoyant force is proportional to the wavelength $2\pi m^{-1}$, whereas the torque associated with the instability restoring force is proportional to m. Hence, to overpower the buoyancy damping m_{cr} increases with α. Also, according to Eq. (39), for $\alpha>90°$ the term f_{BV} contributes to increase the frequency. It is noted that within a completely stable stratified media, the streamwise buoyancy acts also as a restoring force whose associated time is the inverse of the Brunt-Vaisala frequency. At moderate inclinations this restoring force is coupled to the basic hydrothermal mechanism involving a reduction of the oscillation period.

In conclusion, the steady increase of the critical frequency with α (see Fig. 7) is not due to a unique reason and has to be analyzed by quantitatively establishing the relevance of the above introduced mechanisms. Equation (39) has been used for this task. The low-Prandtl-number range is illustrated in Figs. 7(a) and 7(b). In the case of conducting walls [Fig. 7(a)], the inequality $f_{cr}\ll f_\kappa$ holds at least for $\alpha \lesssim115°$; the critical frequency fits well to $0.6f_{Gill}$ and the thermal effects (f_{adv} and f_{BV}) are very small. This situation changes gradually above $115°$ as f_{cr}/f_κ becomes larger than 1 and thermal effects become relevant. The Brunt-Vaisala term, f_{BV}, tends to increase the critical frequency while the cross-stream advection (f_{adv}) tends to decrease it. This latter contribution has been highlighted in Fig. 7, by comparing the outcome of Eq. (39) with an imposed $f_{BV}=0$. In Fig. 7(a), such comparison reveals that at the largest inclinations ($100°<\alpha\lesssim125°$) both thermal contributions are nearly counterbalanced.

A different scenario is found in the case of adiabatic walls. The ratio f/f_κ is greater or roughly equal to 1 for any inclination [see Fig. 7(b)] meaning that the thermal effects need to be considered. For $\alpha<90°$ the (negative) contribution of f_{BV} in Eq. (39) becomes rapidly significant inducing a rather steep decrease of f_{cr}. On the other hand, the effect of cross-stream advection is rather small, so when heating from above, the term f_{BV} is not counterbalanced by f_{adv} (as
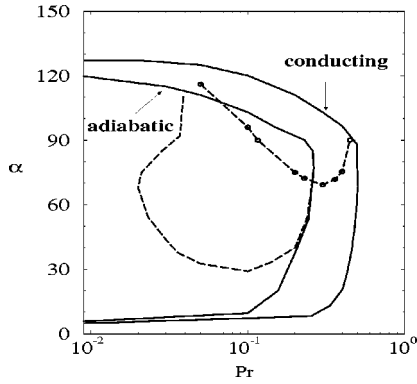
FIG. 8. The region in the Pr-α space where hydrothermal waves are observable (solid lines). Inside the region delimited by dashed lines the critical Rayleigh number of the oscillatory longitudinal disturbance is smaller than that corresponding to transversal shear rolls.

occurs for Bi$\rightarrow\infty$). This implies a further increment of f_{cr} with α. According to Eq. (39) the contribution of f_{BV} is not so large between $90<\alpha<100°$ (about 10% of f_{th}), but it reaches 30% for $\alpha=115°$.

The dependence of f_{cr} with α for moderate values of the Prandtl number Pr≥ 0.1 is displayed in Fig. 7(c) and 7(d). The conclusions extracted above for the low-Prandtl range concerning the dependence on the inclination remain essentially applicable.

Mechanisms for suppression of oscillations

As shown in Fig. 8 the oscillatory instability is damped above a certain (Pr-dependent) cut off inclination. Apart from the stabilization mechanism associated with the cross-stream advection described at the end of Sec. III A, for arbitrarily small Pr, the oscillations can be suppressed owing to another process which dominates at large enough inclination, $\alpha > 95°$. If the cavity is heated from above, the system possesses two different restoring mechanisms acting at different rates: f_{Hart}, which stands for the hydrothermal coupling, and f_{BV} which represents the Brunt-Vaisala frequency associated with the streamwise buoyant force. It has been reckoned that the wave stability is rather sensible to the relation of both frequencies, f_{Hart}/f_{BV}. As illustrated in Fig. 9(a) the ratio f_{Hart}/f_{BV} rapidly decreases for $\alpha>90°$ and it tends to roughly 1 for the largest inclinations, just before the instability is damped. Figure 9(b) shows the value of f_{Hart}/f_{BV} very near to the stabilization angle (1° apart) versus Pr. An interesting result arising from the range Pr<0.1 is that at the stabilization angle the ratio f_{Hart}/f_{BV} becomes slightly smaller than 1 independently of the thermal boundary conditions. On the other hand, as shown in Fig. 9(c), precisely for Pr<0.1, the stabilizing term f_{adv} becomes smaller than f_{BV}, meaning that at low Pr the stabilization is a consequence of the streamwise buoyant force. In order to understand the damping mechanism it is remarked that once f_{BV} becomes larger than f_{Hart}, the restoring buoyant force inverts the sense of the streamwise perturbative flow before the basic cycle of the hydrothermal coupling can be completed,
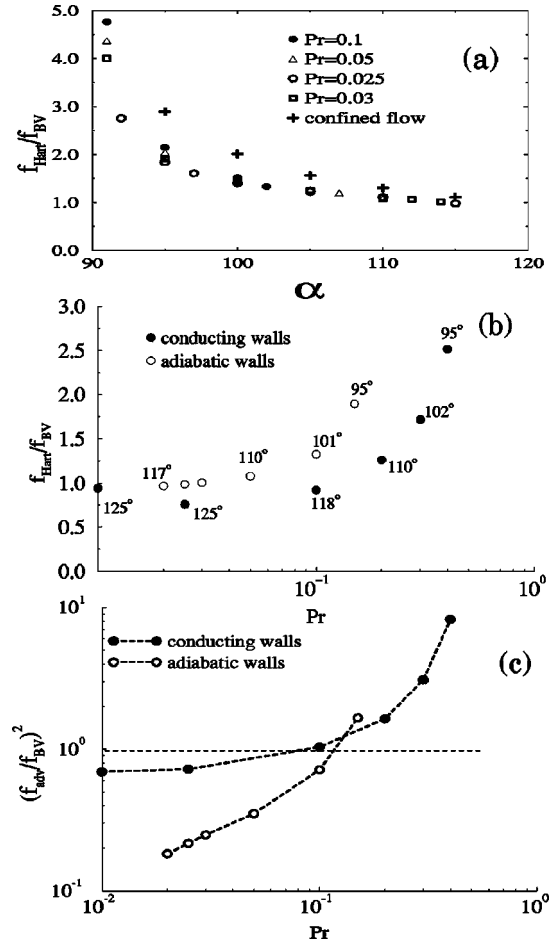
FIG. 9. (a) The value of f_{Hart}/f_{BV} versus the inclination for adiabatic walls. Crosses correspond to numerical calculations for Pr$=0.025$ in a $1\times6\times4$ cavity; the rest of the data arise from the stability analysis in the unbounded domain. (b) The value of f_{Hart}/f_{BV} at an angle one degree smaller than the stabilization angle (indicated for some configurations). (b) The ratio f_{adv}/f_{BV} versus Pr at the same angles than in (b).

thus making impossible the development of the instability. In summary, while for $\alpha<95°$ the oscillations can be only suppressed for Pr$>O(0.1)$ via the cross-stream perturbative advection (see Sec. III A), when using larger inclinations the wave can be damped at arbitrarily small Pr provided that

$$\frac{f_{Hart}}{f_{BV}}=\frac{(R^2 m^2 \sin\alpha \, \mathrm{Pr}^{-1/2}|\widehat{w'_b}|)^{1/3}}{\left(m^2+\dfrac{\pi^2}{3}\right)(R\cos\alpha)^{1/2}}\lesssim 1. \quad (47)$$

In the following section it shall be shown that the above condition also applies in the case of confined flows.

VI. EFFECT OF CONFINEMENT: COMPARISON WITH EXPERIMENTAL DATA AND NUMERICAL CALCULATIONS

In what follows it shall be examined to what extent the theoretical relationships for the frequency are robust with respect to deviations from the plane-parallel assumption in

finite enclosures. These deviations are a consequence of the confinement but also arise owing to the presence of transversal shear rolls, which can coexist with the hydrothermal wave [20]. It should be mentioned that although these effects have been put forward in the previous works to justify the departures of the experimentally measured frequencies from the theoretical trends (see e.g., Refs. [4,6,16]) no quantitative comparison was presented in the case of moderate strongly confined flows.

The validity of Eq. (39) has first been checked by comparison with experiments and numerical calculations done for large aspect ratios. In the case of conducting boundaries, Wang and Korpela [13] reported numerical calculations for a $Pr=0.2$ fluid in a horizontal unbounded configuration. The measured wave number was $m=1.0$ and respectively for $R=R_{cr}=166$ and $R=250$, they reported $f_{cr}=1.87$ and $f=2.44$. The ratio between each of these frequencies and the outcome of Eq. (39) is 1.1, in agreement with the previous comparison with our calculations at $Pr=0.2$ [see Fig. 7(c)].

Almost all previous experiments and numerical calculations considered adiabatic lateral walls. Pratte and Hart [16] made a series of experiments with a $Pr=0.025$ fluid in cavities with different aspect ratios. For the shallowest cavity ($D/H \times L/H = 8 \times 8$) they reported $f \sim Gr^{0.67}$, which agrees with Hart's trend $f_{Hart} \sim Gr^{2/3}$ [see Eq. (46)]. Also, Hung and Andereck [15] made experiments in a $Pr=0.027$ fluid in a very shallow cavity $1 \times 17.7 \times 17.8$, obtaining a wave number $m=0.46$ close to the critical one $m_{cr}=0.38$, and reporting $f=2.15$ at the onset of oscillations (Ra=30.89). The experimentall measured frequencies increased as $f_{exp}=0.035Ra^{2/3}$. Comparison of the experimentally measured frequency with Eq. (46) provides $f_{exp}/f_{Hart} \simeq 0.49$, while Eq. (39) yields $f_{exp}/f_{th} \simeq 0.68$. It is noted that for this particular configuration, the inverse of the characteristic heat diffusion time along one wavelength, $m^2 Pr^{-1/2}/(2\pi) \simeq 0.2$, is more than two times smaller than the oscillation frequency for any value of Ra, hence Hart's assumption remains valid. On the contrary, Gill's trend [Eq. (40)] is clearly inapplicable: $f_{Gill} \sim Ra^{1/2}$.

A. Confined flow

In order to investigate the effect of confinement it is necessary to consider cavities with shorter dimension along the y and z axes. We have performed numerical calculations for $Pr=0.025$ in a $D/H \times L/H = 6 \times 4$ cavity with adiabatic lateral walls, for a range of inclinations, $70° \leq \alpha \leq 115°$. The same system with fixed $\alpha=80°$ was studied in a previous work concerning the interaction of the hydrothermal wave and transversal shear rolls [20]. The interested reader is referred to that paper for numerical details.

In a confined enclosure the hydrothermal wave develops at the core region, away from end regions where the flow turns around [20,22]. Thus it shall be assumed that the fundamental frequency can be estimated by inserting into Eq. (39) the core-averaged Rayleigh number R, and the averaged values of the mean flow profiles, $|\widehat{w'_b}|$, $|\widehat{\theta'_b}|$. We refer to Ref. [20] for details on how these averaged values were calculated from the numerical solution. The following trends are
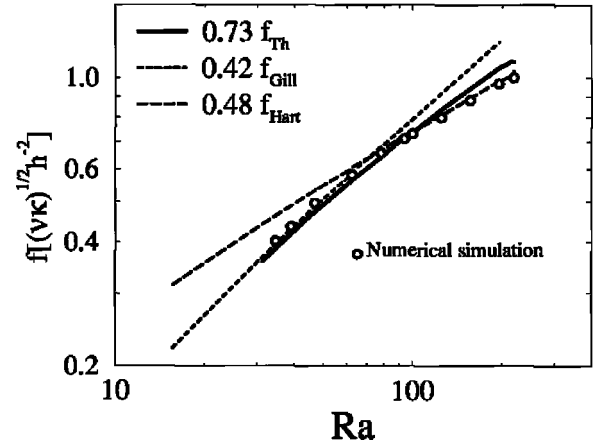
FIG. 10. Comparison of the theoretical trends with the fundamental frequency obtained in the numerical calculations for $Pr=0.025$, $D/H \times L/H = 6 \times 4$ and $\alpha=80°$. All theoretical trends are calculated with core-averaged quantities.

obtained (see [24] for a theoretical derivation): $R=0.27 Ra^{4/7}$, $|\widehat{w'_b}| \simeq 1.2 W_{max}$ (where $W_{max}=0.31 Ra^{3/7}$) and $|\widehat{\theta'_b}| \simeq 0.013$. The evolution of the frequency with Ra was studied for $\alpha=80°$. The outcome of Eq. (39) is compared in Fig. 10 with the fundamental frequency obtained from the numerical calculation of the flow. The agreement is excellent. Quite remarkably, the absolute values of the frequency f_{num} are recovered by $0.73 f_{th}$, in consistency with the previously reported results in the unbounded configuration.

It should be stressed that for all values of the Rayleigh number in Fig. 10, the mean flow is already far from being plane-parallel at the core. The flow grows in complexity through a number of successive transitions reported in Ref. [20]. First, a centered transversal shear roll begins to be formed at Ra$\simeq$15 and it is already well developed at the onset of the oscillations, Ra$\simeq$31. Then, at Ra$\simeq$195 and 218, the flow becomes quasiperiodic and frequency locked to a lower frequency transversal wave formed by a pair of shear rolls. That Eq. (39) (deducted from a linear stability analysis) correctly recovers the trend of the fundamental frequency at the nonlinear-dynamic regime indicates that the basic oscillatory mechanism is not so sensitive, either to the local details of the flow or to the low frequency interaction with the secondary transversal wave. Instead the basic hydrothermal coupling behaves as if it were in a z-independent environment whose properties were those of the averaged mean flow.

An interesting conclusion arising from the confined configuration is comprised of the fact that, as Ra is increased, the wave can cross over the two dynamical regimes described by Eqs. (40) and (46). As seen in Fig. 10, the fundamental frequency does not line up with a unique power law. Instead for Ra$<$60 the frequency fits to Eq. (40), $f_{Gill} \sim Ra^{9/14}$, whereas for larger Ra it lines up with Eq. (46), $f_{Hart} \sim Ra^{3/7}$. Equation (39) correctly predicts the observed change of slope although it slightly overestimates f_{num} at large Ra. It is finally remarked that, quite in consistency with the comments made in Sec. IV, the change of slope occurs

TABLE III. Averaged flow quantities at the core: the local Rayleigh number, R, the maximum streamwise velocity, w_{max} (in κ/h units), the cross-stream temperature gradient, $|\widehat{\theta_b'}|$ [in units of $10^{-2} \times (\Delta T/L) h R$] and the temperature drop between the $x = \pm 1$ $\langle \Delta_x T \rangle$ (in units of ΔT). Data correspond to the numerical calculations made for $Pr = 0.025$ and $Ra = 100$ in a $1 \times 4 \times 6$ cavity. The leftmost columns compare the numerically obtained fundamental frequency f_{num} [in units of $(\nu \kappa)^{1/2}/h^2$] with the TRENDS derived from Eqs. (40), (46), and (39).

α(deg)	R	w_{max}	$\|\widehat{\theta_b'}\|$	$\langle \Delta_x T \rangle$	f_{num}	$\dfrac{f_{num}}{f_{Gill}}$	$\dfrac{f_{num}}{f_{Hart}}$	$\dfrac{f_{num}}{f_{th}}$
76	67.94	4.60	1.08	0.133	0.703	0.37	0.46	0.71
80	66.49	4.39	1.26	0.146	0.732	0.39	0.49	0.73
90	71.00	3.76	1.27	0.151	0.754	0.42	0.51	0.74
95	69.98	3.74	1.08	0.131	0.756	0.43	0.52	0.71
100	71.72	3.61	1.10	0.130	0.78	0.44	0.54	0.72
105	74.56	3.32	1.05	0.126	0.9	0.52	0.63	0.80
115	80.55	2.65	0.93	0.117	0			

when the oscillation frequency becomes larger than the inverse of the characteristic heat diffusion time along one wavelength, $m^2 Pr^{-1/2}/2\pi \sim 0.6$.

B. Varying inclination

Calculations were also carried out for varying inclination at a fixed $Ra = 100$. The obtained values of the fundamental frequency, f_{num}, are shown in Table III along with the relation of f_{num} and the theoretical trends f_{Gill}, f_{Hart}, and f_{th}. First it is noted that both f_{Gill} and f_{Hart} decrease above $\alpha > 90°$ as a consequence of the decrease of the mean flow velocity with the inclination (see Table III). On the contrary, due to the effect of the streamwise buoyancy force f_{num} slightly increases with α. This discrepancy is reflected in f_{num}/f_{Gill} and f_{num}/f_{Hart} (see Table III). On the other hand, Eq. (39) leads to a ratio f_{num}/f_{th} which remains roughly constant around 0.75 for increasing inclination. The good concordance found with the previous comparisons indicates that Eq. (39) correctly takes into account the effect of the streamwise buoyancy on the wave's frequency.

According to the numerical calculations, the oscillations completely disappeared at $\alpha = 115°$. This result is in good agreement with the stabilization angle predicted by the linear stability analysis (116°). More interestingly, as shown in Fig. 9(a), at the transition to the steady flow, the ratio f_{Hart}/f_{BV} has decreased to a value quite close to 1, thus supporting the validity of Eq. (47) for predicting the stabilization.

The evolution of the dynamics and the structure of the flow as the inclination is varied is relatively rich and a more detailed analysis is left for a forthcoming paper. Anyhow, for the sake of consistency, some facts need to be mentioned. When leaning from 80° to 76°, the value of $Ra = 100$ becomes largely supercritical and the flow becomes aperiodic (with a dominant frequency peak at $f \simeq 0.7$). Leaning towards heating-from-above configurations leads to a more interesting dynamic. Above $\alpha = 100°$ the hydrothermal wave frequency becomes about 0.6 times the Brunt-Vaisala frequency $[N_{BV} = (R \cos \alpha)^{1/2}/(2\pi)]$ and it excites an internal gravity wave with a much lower frequency and larger amplitude. After the onset of the internal wave, the amplitude of the hydrothermal wave drastically diminishes in such a way that for $\alpha \geq 105°$ it is no longer trivial to recognize its peak among the multiple harmonics and frequency combinations found in the power spectra. The frequency reported in Table III for 105° corresponds to a relatively larger high-frequency peak, but it is not clear that it matches to the hydrothermal-wave fundamental frequency. Anyhow, at $\alpha = 115°$ the high frequency oscillations associated with the hydrothermal wave vanish, and the internal wave also fades out in absence of the forcing mechanism.

VII. CONCLUDING REMARKS

According to previous analyses [14], hydrothermal waves are responsible for the onset of oscillations in flows of liquid metals $Pr \sim 10^{-2}$. The present study is concerned with the effect of the thermal behavior of the walls and of the cavity inclination on the hydrothermal wave instability of buoyancy-driven convection in end-heated enclosures.

In the first part of the paper, analytical expressions for the neutral curve and dispersion relation were derived by means of a Galerkin procedure. The critical parameters extracted from the analytical approach were shown to quantitatively agree with the exact numerical solution of the perturbative equations. A quite general conclusion arising from the neutral curve is that at the critical Rayleigh number the dominant diffusion rates along the cross-stream (x) and longitudinal (y) directions become comparable. This furnishes a way to estimate the critical parameters, starting from the critical wave number. For $Pr < O(1)$, heat is the fastest diffused quantity along the longitudinal direction at a rate $m^2 Pr^{-1/2}$, independently on the thermal boundary conditions. On the contrary, the thermal behavior of the walls determines the rate of heat diffusion along the depth of the layer (x direction). In conducting walls energy is rapidly diffused along the x direction, at a rate $Pr^{-1/2}$, and the critical mode, $m_{cr} \simeq 1$, enables a balance of the heat fluxes along x and y directions. This yields $R_{cr} \simeq 10^2$ and $f_{cr} \sim 1.6$. In adiabatic walls, the disturbances attain instantaneously a diffusionless temperature profile ($\partial T_p/\partial x = 0$), so momentum is the fastest diffused quantity along the x direction provided that $Pr < 0.1$. Momentum spreads at a rate $(Pr^{1/2})$ which equals the rate of energy diffusion along the y direction; hence $m_{cr} \simeq 2.2 Pr^{1/2}$, $R_{cr} \simeq 10^2 Pr^{1/2}$, and $f_{cr} \sim Pr^{1/2}$. Anyhow, if a small amount of heat flows across the walls ($Bi > Pr$) energy becomes the fastest diffused quantity across the depth of the layer, resulting in an increase of $O(Bi^{1/2})$ in R_{cr}, m_{cr}, and f_{cr}.

The proposed relation for the frequency, derived from the linearized perturbative equations, was shown to correctly forecast the critical frequency in the unbounded geometry and the fundamental frequency measured in previous experiments and hereby presented numerical calculations. On the other hand, the equation recovers the well known theoretical trends for $Pr \ll 1$ derived by Hart [6] and Gill [4], which

respectively arise for frequencies much larger or smaller than the characteristic rate of heat diffusion along one wavelength, $m^2 \text{Pr}^{-1/2}/(2\pi)$. These two limits therefore correspond to the instantaneous heat diffusion regime and the diffusionless regime.

It has been found that the instantaneous diffusion (Gill's) and diffusionless (Hart's) limits are better suited to make estimations of the frequency in respectively conducting and adiabatic walls. Nevertheless, a relevant conclusion of this work is that in general it is necessary to take into account all the contributions of the frequency equation to correctly forecast frequency behavior. For instance, numerical calculations of the oscillatory (Pr=0.025) flow inside a $1\times6\times4$ cavity with adiabatic walls have shown that the behavior of the hydrothermal wave may shift from the fast- to the slow-diffusion trend as Ra is increased. The crossover arises when the fundamental frequency surpasses the heat diffusion rate. This fact is rather probable to occur under moderate or severe confinement because the selected wave number is then larger than the critical one.

Concerning the effect of inclination, when the cavity is tilted towards the vertical position ($\alpha=0°$) the frequency decreases because the unstable stratification tends to maintain unaltered the sense of the streamwise perturbative flow and therefore buoyancy competes with the restoring force. When heating from above, buoyancy acts also as a restoring force along the streamwise direction and the frequency increases. Anyhow, if the buoyant frequency becomes faster than the frequency of the hydrothermal coupling, the sense of the streamwise perturbative flow is reverted before the hydrothermal coupling is able to complete its cycle. As a consequence the oscillation can be damped out at arbitrarily low Pr ($\leqslant 10^{-2}$) providing inclinations around 115°. The condition for stabilization, reflected in Eq. (47), is rather robust in the sense that it holds independently on the thermal boundary conditions, and has been found to be valid under confinement, as revealed by the numerical calculations.

A final point to be stressed is that at the stabilization angle the maximum streamwise velocity remains of the same order than in the oscillatory regime. This fact counterpoints with what happens if the stabilization is achieved via the insertion of a transversal magnetic field (see Refs. [2,7–9]). In this former case the increase of the stability threshold is directly related to the decrease of the mean streamwise velocity. The reason for the different behaviors is that in the inclined setup the damping mechanism acts directly against the perturbative flow. A conclusion to be therefore addressed to the crystal growth community is tilting the convection ampoule may be a simple and suitable way to suppress the thermal oscillations in the Bridgman setup, while still obtaining relatively large transport rates.

[1] C.W. Lan, M.C. Su, and M.C. Liang, J. Cryst. Growth **208**, 717 (2000).
[2] E.J.D.T.J. Hurle and C. Johnson, J. Fluid Mech. **64**, 565 (1974).
[3] F.Z. Haddad, J.P. Garandet, D. Henry, and H.B. Hadid, J. Cryst. Growth **220**, 166 (2000).
[4] A.E. Gill, J. Fluid Mech. **65**, 209 (1974).
[5] J.E. Hart, J. Atmos. Sci. **29**, 687 (1972).
[6] J.E. Hart, J. Fluid Mech. **132**, 271 (1983).
[7] D.H.H. Ben Hadid and S. Kaddeche, J. Fluid Mech. **333**, 23 (1997).
[8] D.H.H. Ben Hadid and S. Kaddeche, J. Fluid Mech. **333**, 57 (1997).
[9] J. Priede and G. Gerbeth, J. Fluid Mech. **404**, 211 (2000).
[10] R.R.S. Benz, P. Hintz, and G.P. Neitzel, J. Fluid Mech. **359**, 165 (1998).
[11] P. Laure and B. Roux, C. R. Acad. Sci., Ser. II: Mec., Phys., Chim., Sci. Terre Univers **305**, 1137 (1987).
[12] H.P. Kuo and S.A. Korpela, Phys. Fluids **31**, 33 (1988).
[13] S.A.K.T. Wang, Phys. Fluids A **1**, 6 (1989).
[14] R. Delgado-Buscalioni, Phys. Rev. E **64**, 016303 (2001).
[15] M.C. Hung and C.D. Andereck, Phys. Lett. A **132**, 253 (1988).
[16] J. Pratte and J.E. Hart, J. Cryst. Growth **102**, 54 (1990).
[17] L. Davoust, R. Moreau, and R. Bolcato, Eur. J. Mech. B/Fluids **18**, 621 (1999).
[18] M. Braunsfurth and T. Mullin, J. Fluid Mech. **327**, 199 (1996).
[19] K.E. McKell, D.S. Broomhead, R. Hones, and D.T.J. Hurle, Europhys. Lett. **12**, 513 (1990).
[20] R. Delgado-Buscalioni, E.C. del Arco, and P. Bontoux, Eur. J. Mech. B/Fluids **20**, 657 (2001).
[21] M. Afrid and A. Zebib, Phys. Fluids A **2**, 1318 (1990).
[22] D. Henry and M. Buffat, J. Fluid Mech. **374**, 145 (1998).
[23] J. Priede and G. Gerbeth, Phys. Fluids **9**, 1621 (1997).
[24] R. Delgado-Buscalioni and E.C. del Arco, Int. J. Heat Mass Transf. **44**, 1947 (2001).
[25] A. Bachran, P. Reinshaus, and W. Seifert, Cryst. Res. Technol. **33**, 1 (1998).
[26] B.L. Markham and F. Rosenberger, J. Cryst. Growth **67**, 241 (1984).
[27] B. Pamplin, in *Crystal Growth*, International Series Sciences Solid State, edited by B. Pamplin (Pergamon, New York, 1980), Vol. 16.
[28] R. Delgado-Buscalioni, Ph. D. thesis, UNED, 1999.